Journal of Magnetism and Magnetic Materials 596 (2024) 171997

Contents lists available at ScienceDirect

Journal of Magnetism and Magnetic Materials

journal homepage: www.elsevier.com/locate/jmmm

Band gap, ferromagnetic resonance and strong microwave absorption of $BaFe_{12-2x}Zn_xSn_xO_{19}$ compounds and enhanced dielectric loss in $BaFe_{12-2x}Zn_xSn_xO_{19}$/carbon nano tube composites

Haozheng Yang [a,1], Zeen Jian [a,1], Kewei Li [b,1], Hong Chang [a,*], Wenyun Yang [b,*], Shunquan Liu [b,*]

[a] School of Physical Science and Technology, Inner Mongolia University, Hohhot, China
[b] School of Physics, Peking University, Beijing, China

ARTICLE INFO

Keywords:
Microwave absorption
Ferrites
Magnetic anisotropy

ABSTRACT

The forbidden bandgap energy, magnetic properties, natural ferromagnetic resonance and microwave absorption are studied on the Zn^{2+} and Sn^{4+} doped $BaFe_{12-2x}Zn_xSn_xO_{19}$. The forbidden band gap of $BaFe_{12-2x}Zn_xSn_xO_{19}$ increases with the increasing doping content x from 1.80 eV up to 1.97 eV. The coercive field, the anisotropy field and the magnetocrystalline constant of $BaFe_{12-2x}Zn_xSn_xO_{19}$ decreases with the increasing doping. The natural ferromagnetic resonance is observed. The high permeability, accompanied with the ferromagnetic resonance, enables strong microwave absorption. $BaFe_{10.4}Zn_{0.8}Sn_{0.8}O_{19}$ has a wide effective microwave absorption bandwidth ($RL \leq -10dB$) of 6 GHz with the material thickness below 2.5 mm in 11.4–17.4 GHz. The dielectric loss has little contribution to the excellent microwave absorption of $BaFe_{12-2x}Zn_xSn_xO_{19}$. The $BaFe_{12-2x}Zn_xSn_xO_{19}$/carbon nanotube (CNT) composites significantly increase the permittivity. The high dielectric loss and the high magnetic loss further improve the microwave absorption. With a very thin thickness of 1.8 mm, $BaFe_{10.4}Zn_{0.8}Sn_{0.8}O_{19}$/CNT has a bandwidth of 7.1 + GHz of 10.9—18 + GHz. With the material thickness thinner than 3 mm, $BaFe_{12-2x}Zn_xSn_xO_{19}$/CNT composites have very broad effective microwave absorption bandwidth of 11.4+, 10.7 and 10.7 GHz, with $x = 0.6$, 0.8 and 1.0, respectively. It illustrates that both $BaFe_{10.4}Zn_{0.8}Sn_{0.8}O_{19}$ and $BaFe_{12-2x}Zn_xSn_xO_{19}$/CNT composites are very promising microwave absorbers.

1. Introduction

As telecommunication enters the 5G and 6G era, the electromagnetic wave pollution in the GHz range is becoming a serious problem worldwide. Many efforts have been done to eliminate the electromagnetic wave pollution. Among them, the microwave absorption materials are a big group. The microwave are composed of rapidly alternating electric and magnetic fields. Therefore, the microwave energy can be consumed by either dissipating the electric energy or the magnetic energy. Generally, the electric energy is consumed by the dielectric materials with enough interfaces, such as the nano materials, Cu_9S_5 [1], graphene@SiO_2@NiO nanoflowers [2], carbon nano fibers @MnO_x [3], Co@C [4], polyaniline@Ba0.5Sr0.5Fe12O19@multi wall carbon nanotubes (MWCNTs) [5]. Carbon nano tubes (CNTs) have very high conductivity. MWCNT/epoxy composite has minimum reflection loss of −15 dB with 3 GHz band width [6]. As an addition, CNTs are effective at improving some composites' microwave absorbing capability, such as silicone oil/CNT [7], MWCNT/Al_2O_3 [8]. With some modification, 10 wt % CNT/$SrFe_{12}O_{19}$/$NiFe_2O_4$ composite have a bandwidth ($RL <$ -10 dB) of 3.27 GHz [9]. CuS/$CoFe_2O_4$/MWCNT composites have a microwave absorption bandwidth of 5.26 GHz at the material thickness of 1.77 mm [10]. ZnO-C wire-in-tubes have an absorption bandwidth of 5.76 GHz [11]. NiCo alloy/carbon nanorod@CNT has an absorption bandwidth of 6.5 GHz with the material thickness of 2.6 mm [12].

Besides the electric energy loss, the microwave energy can also be consumed by the magnetic energy loss. Among them, the ferrites, including the Spinel or the M−type ferrites, are two series being studied most intensively [13–15]. $BaFe_{12-2x}Zr_xNi_xO_{19}$ with $x = 0.6$ has a broad bandwidth of 6.9 GHz [16]. $BaFe_{12}O_{19}$@MnO_2 has an effective absorbing bandwidth of 4.64 GHz [17]. $SrZnCoFe_{16}O_{27}$ has an

* Corresponding authors.
E-mail addresses: Changhong@imu.edu.cn (H. Chang), Yangwenyun@pku.edu.cn (W. Yang), Liushunquan@pku.edu.cn (S. Liu).
[1] Those authors contribute equally to the article.

https://doi.org/10.1016/j.jmmm.2024.171997
Received 26 January 2024; Received in revised form 23 February 2024; Accepted 24 March 2024
Available online 25 March 2024

absorption bandwidth of more than 2.1 GHz [18]. The maximum bandwidth of $Ni_{0.5}Zn_{0.5}Fe_2O_4$ corresponding to $RL \leqslant -10dB$ was 4.6 GHz at 1.71 mm [19]. Around the ferromagnetic resonance (FMR), both the real and the imaginary permeability are very high. It enables strong microwave energy absorption. The natural FMR originates from the magnetocrystalline anisotropy. With very high anisotropy field, $Sr_{1-x/12}Ca_{x/12}Fe_{12-x}Al_xO_{19}$ (x = 1.5–5.5), $Sr_{0.67}Ca_{0.33}Fe_8Al_4O_{19}$ [20–24] have the natural frequencies of FMR above 100 GHz. Instead, in $SrFe_{12-2x}Ni_xRu_xO_{19}$, a strong microwave absorption is observed below 18 GHz [25]. Some studies on the microwave absorbing properties based on FMR are explored, including the $BaFe_{12-y-2x}Al_ySn_xMn_xO_{19}$ M−type hexaferrite [26]. Recently, the magnetic properties have been studied on $SrFe_{12-2x}Zn_xFe_xO_{19}$ [27]. The maximum saturation magnetization and the coercivity are 77 emu/g and 2203 Oe when x = 0.25. Generally, a high magnetization leads to a high permeability. Furthermore, the real part of the complex permeability tells the ability of storing the magnetic energy, and the high imaginary part tells the ability of dissipating the magnetic energy. It inspires us to further study the microwave absorbing properties of the Zn and Sn codoped M−type ferrites. In this paper, we explore the UV–vis spectra, the magnetic properties, and the microwave absorption of $BaFe_{12-2x}Zn_xSn_xO_{19}$ in detail. The $BaFe_{12-2x}Zn_xSn_xO_{19}$ compounds and the $BaFe_{12-2x}Zn_xSn_xO_{19}$/CNT composites have excellent microwave absorption properties with a high magnetic loss and a high dielectric loss.

2. Experiments

The $BaFe_{12-2x}Zn_xSn_xO_{19}$ (x = 0.2, 0.4, 0.6, 0.8 and 1.0) compounds were synthesized by auto combustion method. Stoichiometric amount of $Ba(NO_3)_2$, $Zn(NO_3)_2$, $SnCl_2$, were dissolved in deionized water, respectively. All the solutions were put into one container. Then, the citric acid with the molar ratio of $Ba(NO_3)_2$: citric acid = 1: 1.2 was added and stirred for 2 h. The gel was stirred at 90 °C until a black sticky solid gel was formed. Then, the solid gel was transferred to a beaker, and heated at 180 °C until auto combustion occurred. The powder was sinterred at 1050 °C for 6 h with the heating rate of 5 °C/minute. The MWCNTs were bought from Zhongkeshidai Nano company, China. The outer diameter is in the range of 5——15 nm and the length is about 10——30 μm. The composites of $BaFe_{12-2x}Zn_xSn_xO_{19}$ /MWCNT were prepared with the hydrothermal method. $BaFe_{12-2x}Zn_xSn_xO_{19}$ and MWCNTs were put in an autoclave, and heated at 150 °C for 24 h. The x-ray powder diffraction (XRD) patterns were collected on a Bruker D8 diffractor with the Cu target (K_α = 1.5418 Å). The scanning electronic microscope (SEM) is carried out on JEOL JSM-6400 made in Japan. UV–Vis spectra were recorded in the 200——800 nm domain with a PerkinElmer Lambda750 UV–Vis spectrometer at room temperature. The magnetic properties were measured on a commercial PPMS-9 made in QuantumDesign company with the maximum applied magnetic field of 70 kOe at room temperature. The Agilent N5234A vector network was used to characterize the ferromagnetic resonance and the microwave absorption in 1–18 GHz. The samples used for the microwave absorption were prepared by mixing 80 % of the samples with 20 wt% paraffin wax.

3. Results and discussions

The XRD patterns of the $BaFe_{12-2x}Zn_xSn_xO_{19}$ (x = 0.2, 0.4, 0.6, 0.8 and 1.0) compounds are refined using the Fullprof program with the Rietveld method, as shown in Fig. 1(a). The space group is $P6_3/mmc$. It is the M−type ferrites with some Fe_2O_3 and $BaFe_2O_4$ impurities. In the refinements, the ions' positions are assumed to be the same as in $SrFe_{12-2x}Zn_xSn_xO_{19}$, i.e. 64 % Zn^{2+} and Sn^{4+} being at the 4f1 and 4f2 sites, while the others being at the 2a, 2b and 12 k sites [27]. As shown in Fig. 1(b), the XRD peak moves to the low angle side with the increasing doping content x. It indicates that the lattice constants increase, as shown in Fig. 2. According to the generally accepted Shannon-Prewitt table, the ionic radius of Fe^{3+}, Zn^{2+} and Sn^{4+} ions are 0.49 Å in FeO4

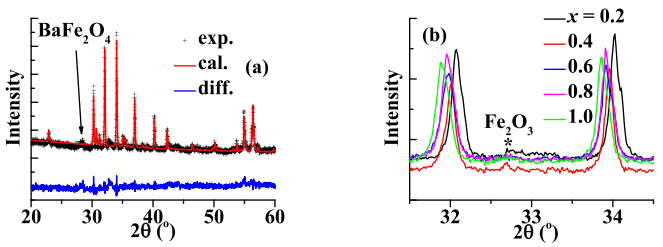

Fig. 1. (a) the refined XRD pattern of the x = 0.4 sample, (b) the XRD patterns of 0.2, 0.4 0.6, 0.8 and 1.0 in the range of $31.5 \leq 2\theta \leq 34.5$.

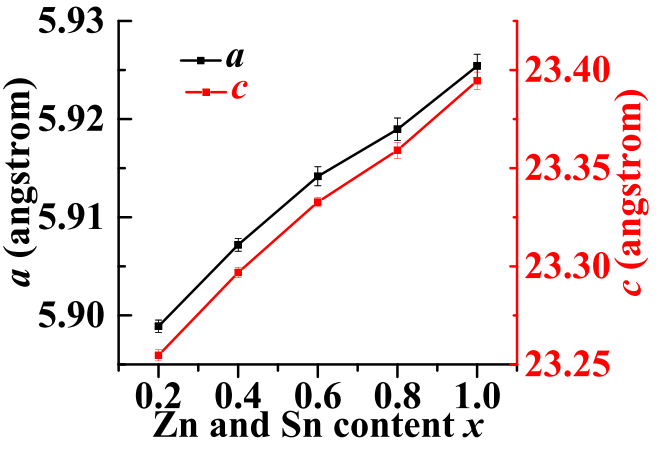

Fig. 2. The lattice constants a and c of $BaFe_{12-2x}Zn_xSn_xO_{19}$.

tetrahedra (or 0.55 Å in the FeO6 octahedra), 0.74 and 0.71 Å, respectively. They are in the order of $Fe^{3+} < Sn^{4+} < Zn^{2+}$. The increasing lattice constants reflect that Zn^{2+} and Sn^{4+} ions are doped in the compounds up to x = 1.0. The particle size is really large, with a diameter more than 5 μm, as shown in Fig. 3.

The UV–vis spectra with a reflection mode are measured on $BaFe_{12-2x}Zn_xSn_xO_{19}$. The Tauc relation describes the relation of the UV–vis absorption and the forbidden band gap E_g [28],

$$\alpha h\nu = K(h\nu - E_g)^n \quad (1)$$

where $h\nu$ is the energy, α is the absorption, K is a constant. The index n is closely related to the transition type. For direct allowed transition, n = 1/2; and it is 3/2, 2 and 4 for direct forbidden transition, indirect allowed and indirect forbidden transition, respectively. $BaFe_{12-2x}Zn_xSn_xO_{19}$ are direct band gap semiconductors [29]. Fig. 4 shows the $(\alpha h\nu)^2$ versus $h\nu$ curves. The band gap E_g is 1.8, 1.87, 1.93, 1.96 and 1.97 eV for the x = 0.2, 0.4, 0.6, 0.8 and 1.0 compounds, respectively. E_g increases with the increasing doping content x. As the doping content approaches x = 1.0, E_g tends to saturate, as shown in Fig. 4(f). It is reported that the band gap energies, E_g, of nano $BaFe_{12}O_{19}$, nano $Ba_{0.5}Sr_{0.5}Fe_{12}O_{19}$ and nano $Ba_{1-x}Ca_xFe_{11.4}Al_{0.6}O_{19}$ are 2.31 eV [30], 2.86 eV [31], and in the range of 1.70 eV and 2.43 eV [32]. E_g varies in a wide range with the doping. It probably indicates that the forbidden bandgap of $BaFe_{12}O_{19}$ is very sensitive to many factors including the particle sizes and the compositions.

The magnetic hysteresis curves are measured with the highest applied field as 70 kOe. The saturation magnetization, defined as the magnetization at 70 kOe, decreases with the increasing doping content x. $BaFe_{12}O_{19}$ and $SrFe_{12}O_{19}$ are ferrimagnetic [20]. The magnetic moments at the 4f1 and 4f2 sites are anti-parallel to those Fe^{3+} ions at the 2a, 2b and 12 k sites. The substitution of the nonmagnetic Zn^{2+} and Sn^{4+} may increase or decrease the magnetization. It depends on their occupation sites. Previously, it was reported that in $SrFe_{12-2x}Zn_xSn_xO_{19}$, 64 %

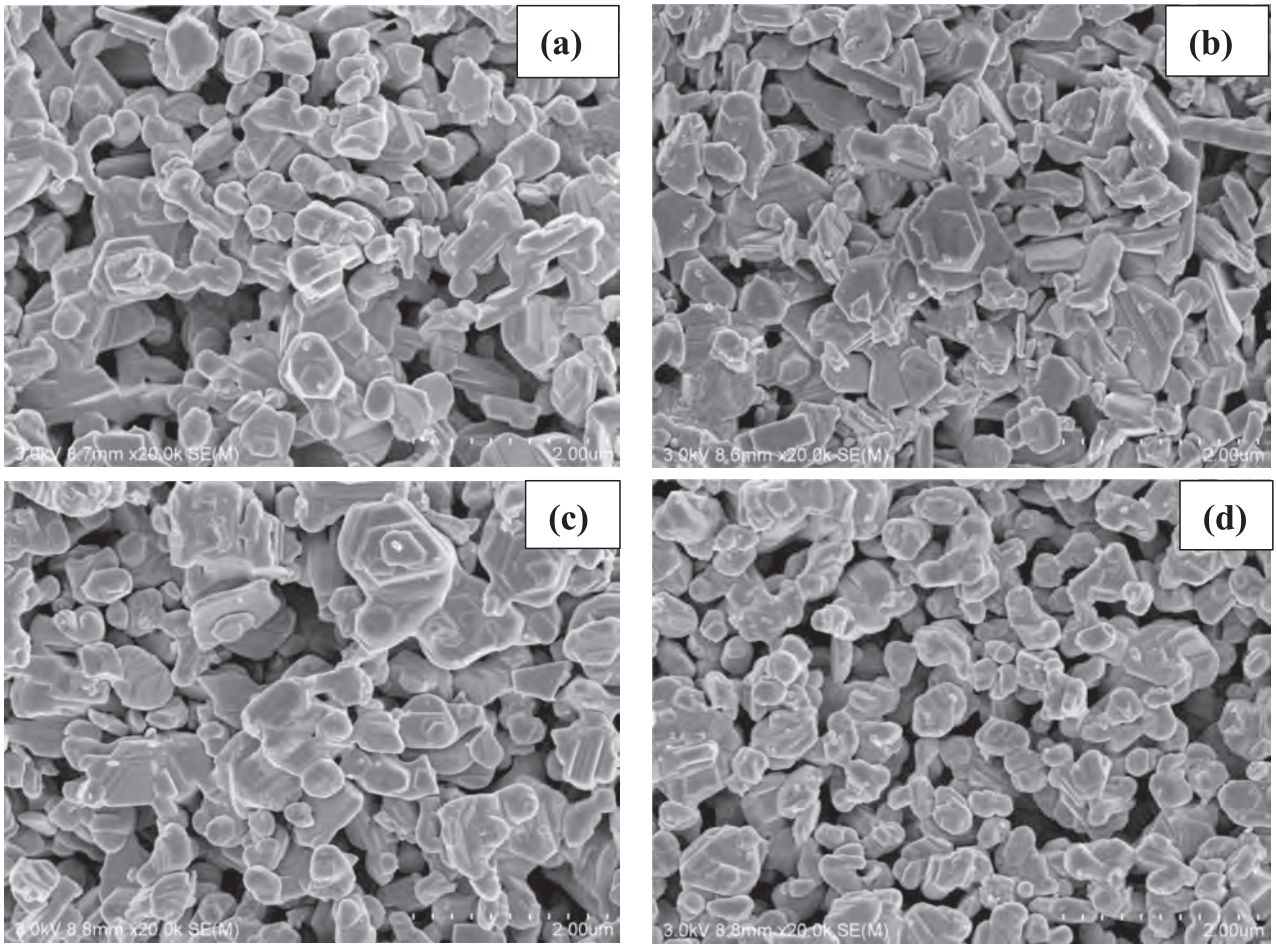

Fig. 3. SEM image of the (a) $x = 0.4$, (b) $x = 0.6$, (c) $x = 0.8$, (d) $x = 1.0$ compounds.

Zn^{2+} and Sn^{4+} being at the 4f1 and 4f2 sites, while the others being at the 2a, 2b and 12 k sites [27]. Therefore, with the increasing doping content x, the saturation magnetization should increase. It is different from the measurements. It is probably due to the nonlinear alignment of the magnetic moments, similar to that is in $SrFe_{12-2x}Zn_xSn_xO_{19}$ [27]. The nonmagnetic Zn^{2+} and Sn^{4+} ions drive the alignment of the magnetic moments become canted. As shown in Fig. 5(a), as a result of the canted alignment of the $x = 0.4$, 0.6, 0.8 and 1.0 compounds, the magnetization keeps increasing even at the applied magnetic field as high as 70 kOe. The coercive field H_c rapidly decreases with the increasing doping content x from 4.01 kOe in $x = 0.2$ down to 56.4 Oe in $x = 1.0$. Because the annealing is carried out at the temperature as high as 1050 °C for 6 h, the particles are very large, with the diameter more than 5 μm. All of them are not single magnetic domains. The coercive field H_c reflects the variation of H_a, but is much smaller than H_a.

In Fig. 6, the real and imaginary parts, μ' and μ'', of the magnetic permeability are shown. There are two resonance peaks in the $x = 0.2$ compound, at 1.2 and 17.0 GHz, respectively. The one at the low frequency gradually decreases with the increasing doping content x, and it is at 0.7 GHz in $x = 1.0$. In the study of the reaction dynamics, it is reported that α-Fe_2O_3 and $BaFe_2O_4$ naturally exist as intermediate phases before the formation of the M−type Ba ferrites [29–32]. Generally, the spinel ferrite has a low anisotropy field, the FMR frequency is in the MHz range. It is reasonable to assume that $Ba(Fe,Zn,Sn)_2O_4$ produces the resonance below 1.2 GHz. At high frequency, both the permeability and the permittivity have a resonance. It is probably due to the electric dipole oscillation, which can radiate electromagnetic wave.

In the $x = 0.6$, 0.8 and 1.0 compounds, both μ' and μ'' have a wide hump, and the peak of the μ'' hump is at the half maximum of the μ' hump. It clearly indicates that the wide hump is due to the FMR. The natural frequency (f_r) of FMR is 16.4, 12.5 and 8.6 GHz in $x = 0.6$, 0.8 and 1.0, respectively. It linearly decreases with x. As discussed above, the coercive field H_c also linearly decreases from $x = 0.4$ to 1.0, and both H_c and f_r are proportional to H_a. The linear extrapolation gives a reasonable value of $f_r = 20.5$ GHz in $x = 0.4$, as listed in Table 1. The natural FMR originates from the magnetocrystalline anisotropy. f_r and H_a has the relation, $f_r = \gamma H_a = 1.4gH_a$, with $\gamma = qg\mu_0/2m_e$, g as the g-factor, q, m_e and μ_0 as the electron charge, the electron mass and the magnetic permeability of the vacuum, respectively. The increasing doping content x decreases f_r and also H_a, as listed in Table 1. The magnetocrystalline anisotropy constant K_1 is deduced from $H_a = \frac{2K_1}{\rho M_s}$. The Zn^{2+} and Sn^{4+} doping seriously deteriorates K_1. Compared with $SrFe_{12-x}Ga_xO_{19}$, K_1 of $BaFe_{12-2x}Zn_xSn_xO_{19}$ decreases much faster with x [33]. The magnetocrystalline anisotropy is a complex function of the valence state of Fe^{3-d} ions, the noncentral symmetry at some Fe-O polyhedra [20], and also the nonmagnetic ions' doping.

In the microwave absorption, the real part of the permeability reflects the capability of storing the magnetic energy, and the imaginary part indicates the dissipating capacity. The big humps observed in μ' and μ'' provide high storing and high dissipating capacity of the microwave energy. It indicates strong absorption of the microwave energy. The magnetic tangent loss $\tan\delta_\mu = \frac{\mu''}{\mu'}$ denotes the capability of consuming the magnetic energy of the microwave. As shown in Fig. 6(f), $\tan\delta_\mu = \frac{\mu''}{\mu'}$ is obviously higher in the $x = 0.6$, 0.8 and 1.0 compounds than their peer $x = 0.2$ and 0.4 compounds. It is largely due to the contribution of the big hump originating from the FMR. The highest $\tan\delta_\mu = 0.45$ is in $x =$

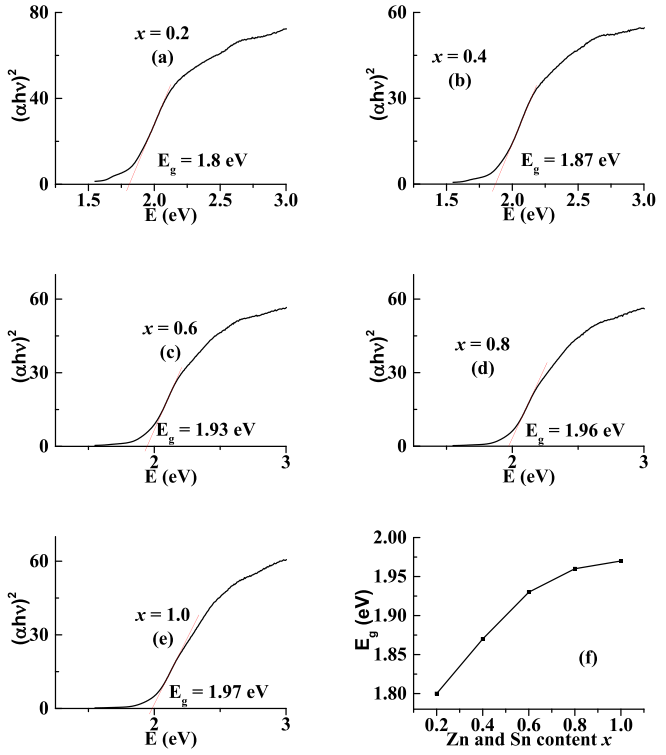

Fig. 4. $(\alpha h\nu)^2$ versus $h\nu$ curves of $BaFe_{12-2x}Zn_xSn_xO_{19}$ with (a) $x = 0.2$, (b) $x = 0.4$, (c) $x = 0.6$, (d) $x = 0.8$ and (e) $x = 1.0$, and (f) the band gap energy E_g versus the doping content x.

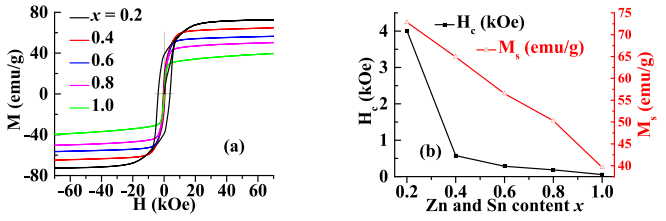

Fig. 5. (a) the hysteresis curves of $BaFe_{12-2x}Zn_xSn_xO_{19}$ ($x = 0.2$, 0.4, 0.6, 0.8 and 1.0), (b) the variation of the coercive field H_c and the saturation magnetization M_s with the Zn and Sn doping content x.

0.6, and it moves to the low frequency side in $x = 0.8$ and 1.0 with $\tan\delta_\mu = 0.4$.

The dielectric permittivity is shown in Fig. 7, with ε' and ε'' as the real and the imaginary parts, respectively. Similar to the permeability, the real part of the permittivity denotes the capability of storing the electric energy, and the imaginary part tells the capability of dissipating the electric energy. Except for the rapidly decreasing ε' and ε'' below 2 GHz in $x = 0.2$, 0.4, 0.6 and 0.8, ε'' is close to zero in all the compounds. It indicates that the dielectric loss is rather low.

In the microwave absorption, the impedance matching plays an important role. It is calculated with the equation

$$Z_{in} = Z_0\sqrt{\frac{\mu_r}{\varepsilon_r}}\tanh[j\frac{2\pi fd}{c}\sqrt{\mu_r\varepsilon_r}] \quad (5)$$

where Z_{in} and Z_0 as the material and the free air impedance, respectively, μ_r and ε_r as the complex permeability and permittivity, respectively, f as the frequency and d as the material thickness. As $\frac{Z_{in}}{Z_0}$ is close to 1, the microwave is able to fully enter the material. As $\frac{Z_{in}}{Z_0}$ deviates from 1 very far, the microwave is reflected back into the air. As shown in Fig. 8, the range with $0.5 \leqslant \frac{Z_{in}}{Z_0} \leqslant 1.5$ is highlighted with the dark blue, light blue,

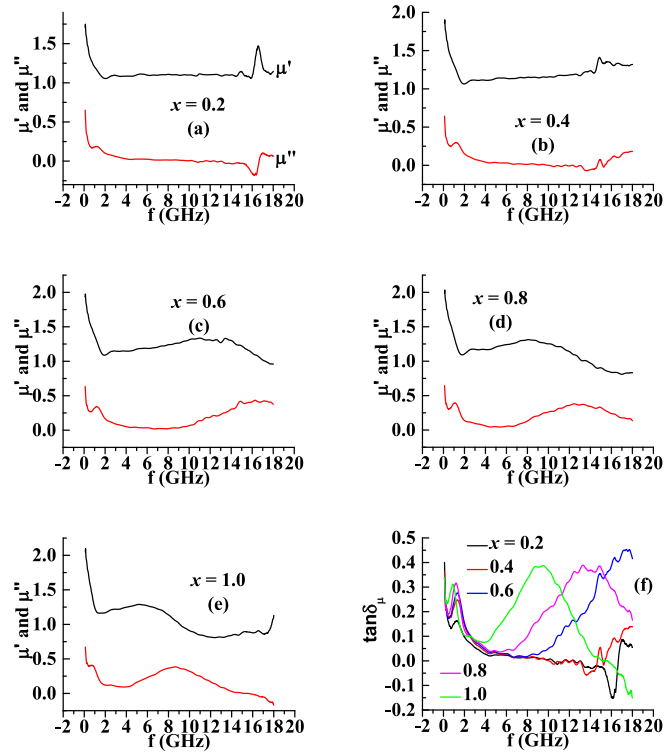

Fig. 6. The real and imaginary parts, μ' and μ'', of the magnetic permeability of $BaFe_{12-2x}Zn_xSn_xO_{19}$ with (a) $x = 0.2$, (b) $x = 0.4$, (c) $x = 0.6$, (d) $x = 0.8$ and (e) $x = 1.0$, and (f) the magnetic tangent loss $\tan\delta_\mu$ versus the doping content x.

green and brown. In the $x = 0.4$ compound, with $4mm \leqslant d \leqslant 6mm$, the frequency range of $0.5 \leqslant \frac{Z_{in}}{Z_0} \leqslant 1.5$ is above 16 GHz. In $x = 0.6$, with the thickness between 1 and 3 mm, $0.5 \leqslant \frac{Z_{in}}{Z_0} \leqslant 1.5$ is in the frequency range of 15—18 GHz. In $x = 0.8$, $0.5 \leqslant \frac{Z_{in}}{Z_0} \leqslant 1.5$ is in a wide frequency range of 13–16 GHz with the thickness of 1.2–3.5 mm. Compared to the $x = 0.8$ compound, the $x = 1.0$ compound has a shrinking frequency range, but still covers a wide 7–11.5 GHz frequency range with the thickness below 6 mm.

A good microwave absorption is expected with a good impedance matching. The microwave absorption is defined by the reflection loss (RL). It is calculated with the equation

$$RL = 20\log\frac{Z_{in} - Z_0}{Z_{in} + Z_0} \quad (6)$$

Herein, the effective absorption is defined as $RL \leqslant -10dB$, with more than 90 % microwave energy being consumed. In Fig. 9, the variation of RL with the thickness and the frequency is shown. Because the $x = 0.2$ compound does not have good microwave absorption, it is not shown in Fig. 9. In $x = 0.4$, the effective absorption has 2 parts, i.e. in 16—18 + GHz with the thickness of 4.2—5.5 mm, and in 8.6—11.6 GHz above 7.2 mm. The second stripe with $RL \leqslant -10dB$ in $x = 0.4$ is above 7.1 mm in 14–18 + GHz.

In $x = 0.6$, there are 3 stripes of absorption below 9.9 mm and in the frequency range of 1–18 GHz. The first one has a bandwidth of 3.6 + GHz with a very thin thickness of 1.4–2.1 mm in 14.4—18 + GHz. At a single layer thickness of 2 mm, the effective absorption band is in 14.4—18 + GHz with a bandwidth of 3.6 + GHz. Another two stripes are at thick material thicknesses above 4.8 mm. In $x = 0.8$, there are 2 stripes. The one at thin thickness of 1.9–2.5 mm has a bandwidth of 6 GHz in 11.4–17.4 GHz. The single layer absorption band at 2.2 mm has a bandwidth of 5 GHz in 12–17 GHz. In $x = 1.0$, there are 2 absorption stripes. The one between the thickness of 2.7–3.9 mm covers the frequency of 7.9–11.8 GHz.

Table 1
The lattice parameters a and c, the saturation magnetization (M_s), and the coercive field (H_c), the NFMR frequency (f_r), the anisotropy field (H_a) and the magneto-crystalline constant K_1 (erg/cm^3) of $BaFe_{12-2x}Zn_xSn_xO_{19}$.

x	a(Å)	c(Å)	H_c(kOe)	M_s(emu/g)	f_r(GHz)	H_a (kOe)	K_1(erg/cm^3)
0.2	5.89889	23.25469	4.01	72.84			
0.4	5.9072	23.29688	0.578	64.9	20.5	7.32143	1.27857
0.6	5.91417	23.33274	0.2846	56.5	16.4	5.85714	0.89827
0.8	5.91897	23.35914	0.1868	50.3	12.5	4.46429	0.61548
1	5.92541	23.39454	0.0564	39.6	8.6	3.07143	0.33626

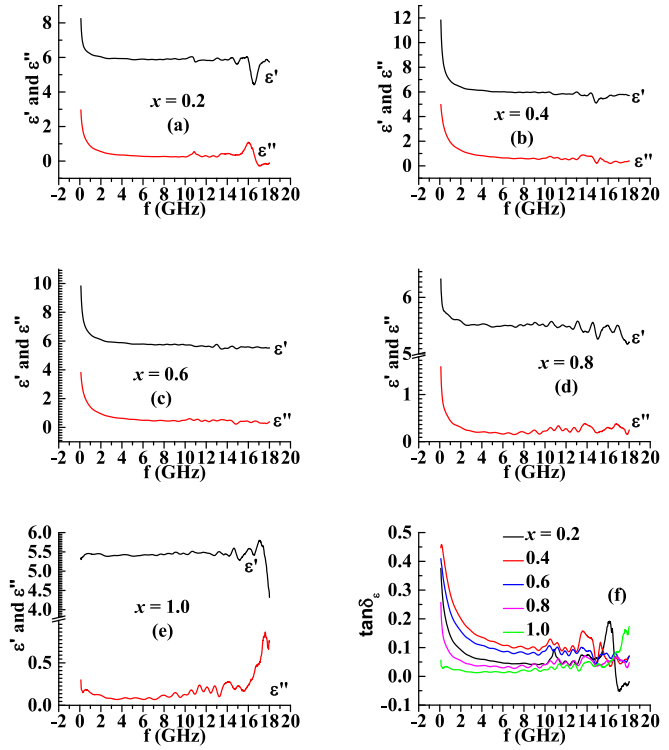

Fig. 7. The real and imaginary parts, ε' and ε'', of the dielectric permittivity of $BaFe_{12-2x}Zn_xSn_xO_{19}$ with (a) $x = 0.2$, (b) $x = 0.4$, (c) $x = 0.6$, (d) $x = 0.8$ and (e) $x = 1.0$, and (f) the dielectric tangent loss $\tan\delta_\varepsilon$ versus the doping content x.

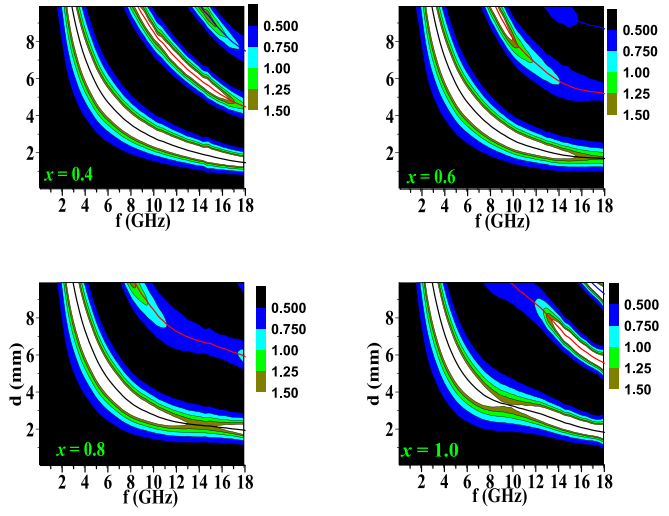

Fig. 8. The impedance matching $\frac{Z_{in}}{Z_0}$ of $BaFe_{12-2x}Zn_xSn_xO_{19}$ with (a) $x = 0.4$, (b) $x = 0.6$, (c) $x = 0.8$, (d) $x = 1.0$ at the different material thickness and frequency, the lines are calculated from the quarter wavelength criteria.

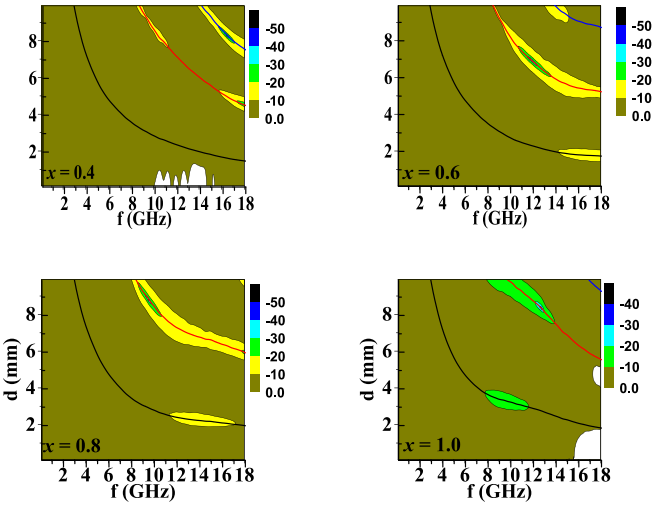

Fig. 9. RL of $BaFe_{12-2x}Zn_xSn_xO_{19}$ with (a) $x = 0.4$, (b) $x = 0.6$, (c) $x = 0.8$, (d) $x = 1.0$ at the different material thickness and frequency, the lines are calculated from the quarter wavelength criteria.

Noticed that in all the compounds, the absorption has several stripes, it is due to the quarter wavelength criteria. Supposed that the material has a metal bottom. As the microwave radiates toward the material, part of the microwave is reflected back into the air and part enters the material. As the microwave meets the metal bottom, it is reflected back and enters the air again. If the two beams in the air are exactly anti phase, the overall microwave is canceled. It demands the material thickness is $\lambda/4$ or odd times $\lambda/4$. It is called the quarter wavelength criteria. The optimum thickness satisfying the quarter wavelength criteria fulfills the equation

$$d_m = \frac{nc}{4f_m\sqrt{|\mu_r\varepsilon_r|}} \tag{7}$$

In Figs. 8 and 9, the calculated optimum thickness at corresponding frequency is shown as the black, red and blue lines. As shown in Fig. 8, the range with $0.5 \leqslant \frac{Z_{in}}{Z_0} \leqslant 1.5$ is around the optimum thickness. Both the good impedance matching and the quarter wavelength criteria enable good microwave absorption. As shown in Fig. 9, the range with $RL \leqslant -10dB$ is around the optimum thickness of the quarter wavelength criteria.

In order to further study the factors determining RL, Fig. 10 is drawn with RL, μ'', the optimum thickness d_m, and $|\frac{Z_{in}}{Z_0}|$. In $x = 0.4$, at $d = 4.6$ mm and 17.8 GHz, the minimum RL is RL_{min} = -26 dB with a comparatively high $\mu'' = 0.19$. The optimum thickness of the quarter wavelength criteria is exactly at $d_m = 4.6$ mm, and $|\frac{Z_{in}}{Z_0}| = 1.1$. The minimum RL is a combining effect of μ'', d_m, and $|\frac{Z_{in}}{Z_0}|$. In the $x = 0.6$ compound, with the material thickness 2 mm (different from the optimum $d_m = 1.8$ mm), $RL_{min} = -12$ dB. $\mu'' = 0.44$ is high, and $|\frac{Z_{in}}{Z_0}| = 1.18$. Similar to $x = 0.6$, the $x = 0.8$ and 1.0 compounds have a high $\mu'' = 0.38$, but the material thickness is not the optimum one. The high μ'' results in the wide

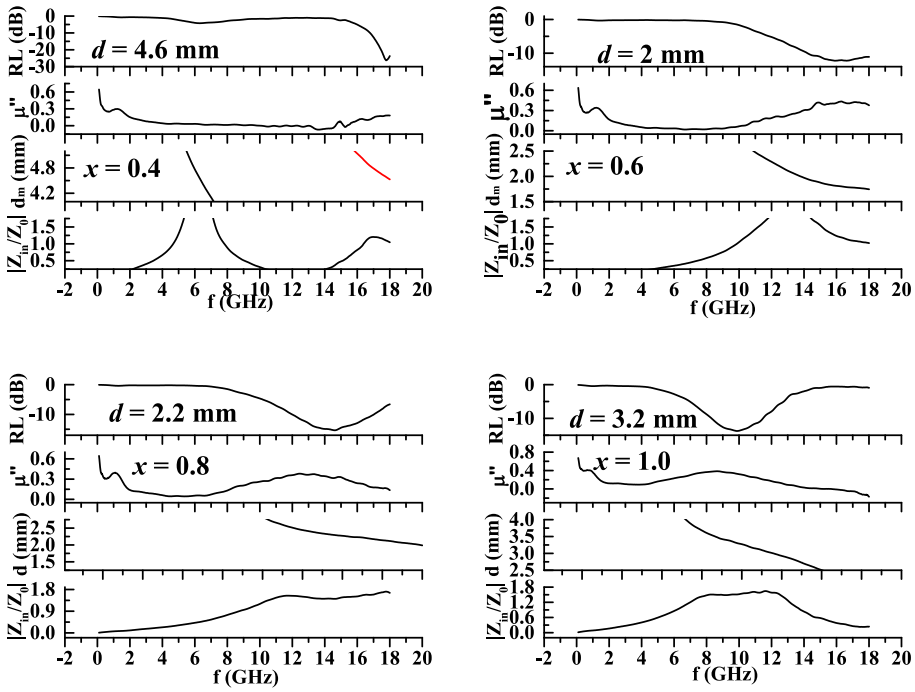

Fig. 10. *RL* of $BaFe_{12-2x}Zn_xSn_xO_{19}$ with (a) $x = 0.4$, (b) $x = 0.6$, (c) $x = 0.8$, (d) $x = 1.0$ at the different material thickness and frequency, the lines are calculated from the quarter wavelength criteria.

absorption bands in $x = 0.6$ at 2 mm, in $x = 0.8$ at 2.2 mm, and in $x = 1.0$ at 3.2 mm. If only $|\frac{Z_{in}}{Z_0}|$ is good enough, a high μ'' dissipates the microwave energy, even when the quarter wavelength criteria is not fulfilled.

As shown above, the microwave absorption is mainly contributed by high magnetic absorption. The dielectric loss is very low. In order to further increase the microwave absorption, $BaFe_{12-2x}Zn_xSn_xO_{19}$/carbon nanotube (CNT) composites are prepared with the hydrothermal method. The real and imaginary parts of the magnetic permeability, μ' and μ'' of the $x = 0.6$, 0.8 and 1.0 compounds and the $BaFe_{12-2x}Zn_xSn_xO_{19}$/CNT composites are shown in Fig. 11. The addition of CNT does not change μ' and μ'' very much.

The $BaFe_{12-2x}Zn_xSn_xO_{19}$ compounds have very low ε''. Compared with the compounds, the $BaFe_{12-2x}Zn_xSn_xO_{19}$/CNT composites have much higher$\varepsilon'' = 3.4$, 1.8, 2.4 in the composites with $x = 0.6$, 0.8 and 1.0, as shown in Fig. 12. The high ε'' means that the dissipating capacity is greatly enhanced by the addition of the CNTs. As shown in Fig. 13, the Cole-Cole curves have long tails in the composites with $x = 0.6$, 0.8 and 1.0. It supports that the highly conductive CNT introduce leakage

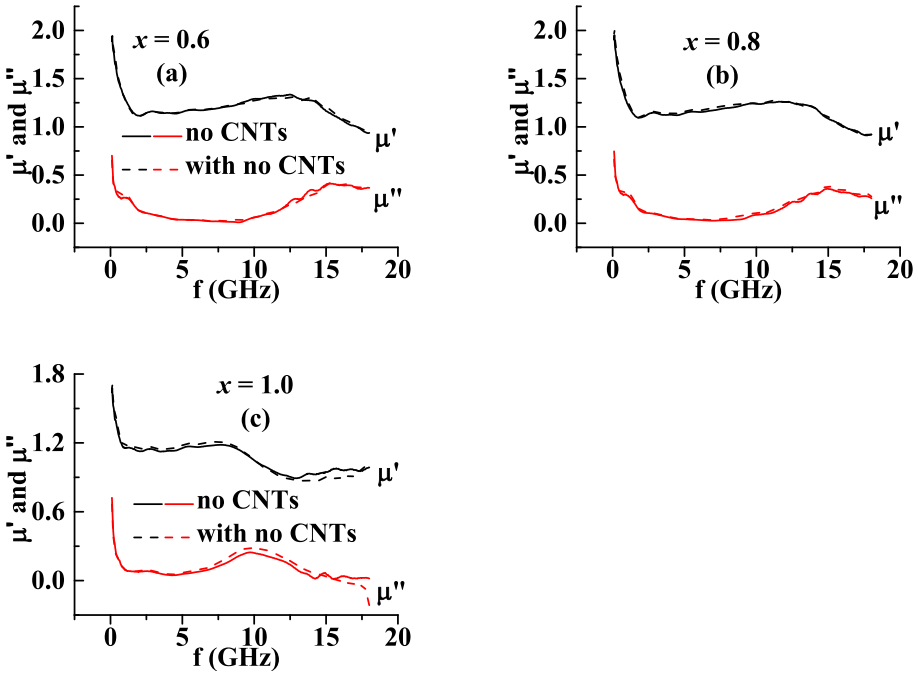

Fig. 11. μ' and μ'' of the $BaFe_{12-2x}Zn_xSn_xO_{19}$/CNT composites with (a) $x = 0.6$, (b) $x = 0.8$, (c) $x = 1.0$.

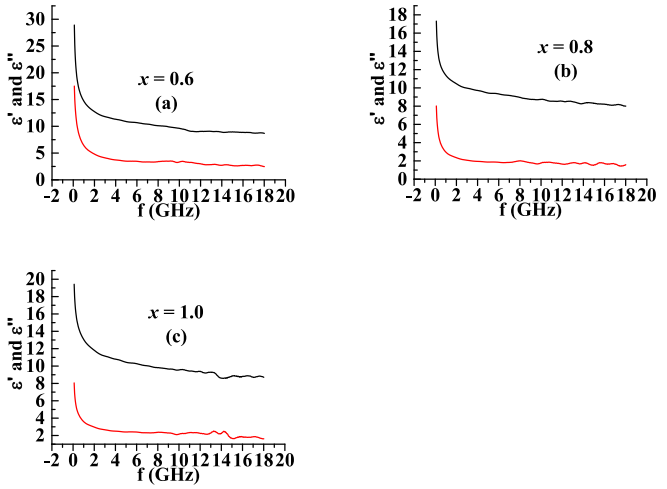

Fig. 12. ε' and ε'' of the $BaFe_{12-2x}Zn_xSn_xO_{19}$/CNT composites with (a) $x = 0.6$, (b) $x = 0.8$, (c) $x = 1.0$.

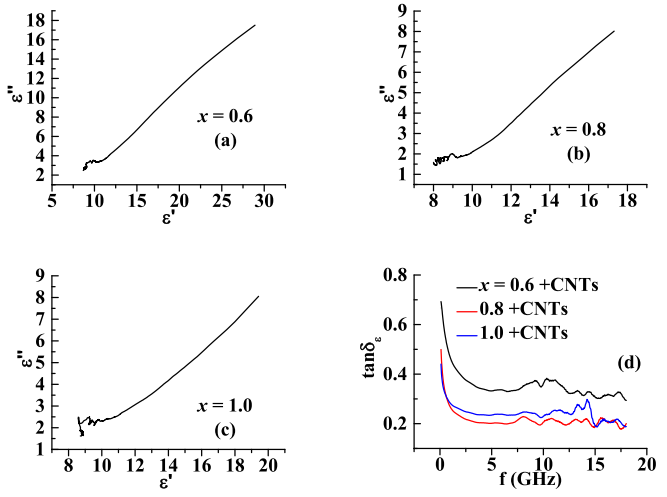

Fig. 13. The Cole-Cole curves, $\varepsilon' \sim \varepsilon''$, of the $BaFe_{12-2x}Zn_xSn_xO_{19}$/CNT composites with (a) $x = 0.6$, (b) $x = 0.8$, (c) $x = 1.0$, and (d).

conduction. As a result of the enhanced ε' and ε'', the dielectric tangent loss $\tan\delta_\varepsilon = \frac{\varepsilon''}{\varepsilon'}$ of the composites becomes significantly higher than their peer compounds, as shown in Fig. 13(d).

As mentioned above, the $BaFe_{12-2x}Zn_xSn_xO_{19}$ compounds have high magnetic loss with a high μ'' due to the FMR. The $BaFe_{12-2x}Zn_xSn_xO_{19}$/CNT composites keep the high magnetic loss. At the same time, the dielectric dissipation increases in the $BaFe_{12-2x}Zn_xSn_xO_{19}$/CNT composites due to the increased ε''. Therefore, the $BaFe_{12-2x}Zn_xSn_xO_{19}$/CNT composites are expected to have a very strong microwave absorption. As shown in Fig. 14, below 3 mm, the composites with $x = 0.6$, 0.8 and 1.0 have very broad absorption bands of 6.6——18 + GHz, 7.3——18 + GHz, and 6.1——17.3 GHz, respectively. The bandwidths are 11.4, 10.7 and 11.2 GHz, respectively. As for a single layer absorption, at 1.8 mm, the composite with $x = 0.8$ has a broad bandwidth of 7.1 + GHz from 10.9 to 18 + GHz. As for RL < -5 dB, at the material thickness of 1.2 mm, the composite with $x = 0.8$ has the bandwidth of 6.4 + GHz in 11.6–18 + GHz. In Table 2, RL are compared with the compounds from the latest highly honored publications. $BaFe_{10.8}Zn_{0.6}Sn_{0.6}O_{19}$/CNT and $BaFe_{10.4}Zn_{0.8}Sn_{0.8}O_{19}$/CNT have very broad effective microwave absorption at very thin thickness. They are very competitive microwave absorbers.

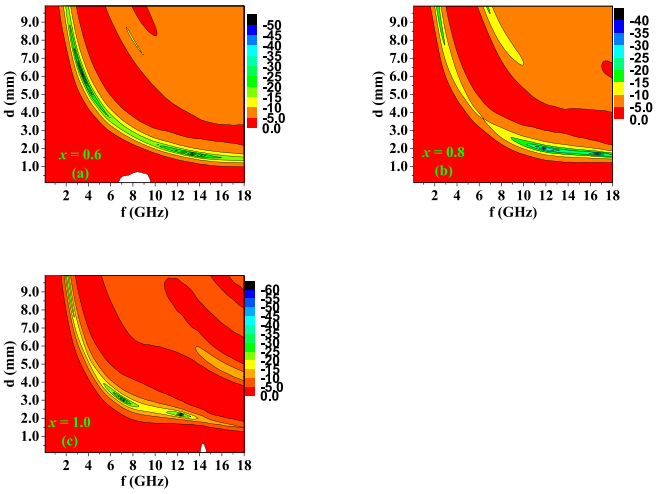

Fig. 14. RL of the $BaFe_{12-2x}Zn_xSn_xO_{19}$/CNT composites with (a) $x = 0.6$, (b) $x = 0.8$, (c) $x = 1.0$.

Table 2
The comparison of the microwave absorption properties, at the absorber thickness d (mm), the microwave absorption bandwidth BW (GHz), the absorption frequency band (GHz), and the references.

	d (mm)	BW (GHz)	Band (GHz)	Ref.
$BaFe_{10.8}Zn_{0.6}Sn_{0.6}O_{19}$/CNT	3	11.4+	6.6——18+	Present work
$BaFe_{10.4}Zn_{0.8}Sn_{0.8}O_{19}$/CNT	3	10.7	7.3——18+	Present work
$BaFe_{10}ZnSnO_{19}$/CNT	3	11.2	6.1——17.3	Present work
$BaFe_{10.4}Zn_{0.8}Sn_{0.8}O_{19}$/CNT	1.8	7.1+	10.9——18+	Present work
$BaFe_{10.4}Zn_{0.8}Sn_{0.8}O_{19}$	2.5	6	11.4–17.4	Present work
$SrFe_{10.6}Ni_{0.7}Ru_{0.7}O_{19}$	2.1	8.8+	9.20——18+	[25]
$SrFe_{11.0}Ni_{0.5}Ru_{0.5}O_{19}$	2.1	11.31+	6.69 to 18+	[25]
Fe_3O_4/graphene	3.5	4.3	7.5–11.8	[34]
Nano TiO_2/$BaFe_{12}O_{19}$	2.4	4.5	6–10.5	[35]
Nano $BaTiO_3$	2	1.7	13.3–15	[36]
$Ba_{0.5}Sr_{0.5}Co_{0.2}Al_{0.2}Fe_{11.6}O_{19}$	1.5	3.27	9.23–12.5	[37]
Ag_3PO_4 nanorod/$SrFe_{12}O_{19}$	3	10.5+	7.5–18+	[38]

4. Conclusion

The forbidden energy band gap of $BaFe_{12-2x}Zn_xSn_xO_{19}$ increases with the increasing doping content x from 1.80 eV up to 1.97 eV. The coercive field, the saturation magnetization and the anisotropy field decrease with the increasing doping content x. Strong natural ferromagnetic resonances are observed in the $x = 0.4$, 0.6 and 1.0 compounds. The high imaginary part of the permeability induces the strong microwave absorption. $BaFe_{10.4}Zn_{0.8}Sn_{0.8}O_{19}$ has a wide effective microwave absorption bandwidth ($RL \leqslant -10dB$) of 6 GHz with the material thickness below 2.5 mm in 11.4–17.4 GHz.

The $BaFe_{12-2x}Zn_xSn_xO_{19}$/CNT composites have both high permittivity and high permeability. The microwave absorption further improves. With the material thickness thinner than 3 mm, $BaFe_{12-2x}Zn_xSn_xO_{19}$/CNT composites have very broad effective microwave absorption bandwidth of 11.4+, 10.7 and 10.7 GHz, with $x = 0.6$, 0.8 and 1.0, respectively. With a very thin thickness of 1.8 mm, $BaFe_{10.4}Zn_{0.8}Sn_{0.8}O_{19}$/CNT has a bandwidth of 7.1 + in 10.9–18 + GHz. It illustrates that the $BaFe_{12-2x}Zn_xSn_xO_{19}$/CNT composites are promising microwave absorbers.

5. Author statements

Ms. Haozheng Yang, Mr. Zeen Jian and Mr. Kewei Li prepared the samples and measured the experimental data. Dr. Shunquan Liu and Dr. Wenyun Yang provided valuable discussion. Dr. Hong Chang designed the experiments and wrote the manuscript.

CRediT authorship contribution statement

Haozheng Yang: Data curation. **Zeen Jian:** Data curation. **Kewei Li:** Data curation. **Hong Chang:** Writing – original draft, Funding acquisition, Formal analysis, Conceptualization. **Wenyun Yang:** Formal analysis. **Shunquan Liu:** Funding acquisition, Formal analysis.

Declaration of competing interest

The authors declare that they have no known competing financial interests or personal relationships that could have appeared to influence the work reported in this paper.

Data availability

Data will be made available on request.

Acknowledgments

This work is financially supported by the National Natural Science Foundation of China (Grant No. 11864027), Natural Science Foundation of Inner Mongolia (Grant No. 2020MS01019), Key Technology Research and Development of Inner Mongolia (2020GG0162). The zhong-ke-bai-ce company provides technical support of magnetic and XRD measurements.

References

[1] F.J. Tao, M. Green, A.T.V. Tran, Y.L. Zhang, Y.S. Yin, X.B. Chen, Plasmonic Cu_9S_5 nanonets for microwave absorption, ACS Appl. Nano Mater. 2 (2019) 3836.
[2] L. Wang, Y. Huang, X. Ding, P.B. Liu, M. Zong, Ternary nanocomposites of graphene@SiO2@NiO nanoflowers: synthesis and their microwave electromagnetic properties, Micro & Nano Lett. 8 (2013) 391.
[3] X.F. Xu, S.H. Shi, G.P. Wan, C.C. Hao, Z.Y. He, G.Z. Wang, Uniformly coating MnO_x nanoflakes onto carbon nanofibers as lightweight and wideband microwave absorbers with frequency-selective absorption, Mater. Design 183 (2019) 108167.
[4] Y.X. Li, J.Y. Wang, R.G. Liu, X.N. Zhao, X.J. Wang, X.F. Zhang, G.W. Qin, Dependence of gigahertz microwave absorption on the mass fraction of co@c nanocapsules in composite, J. Alloy. Compd. 724 (2017) 1023.
[5] Y. Cao, A.M. Mohamed, A. Sharifi, M.N. Akhtar, Microwave absorption characteristics of polyaniline@Ba0.5Sr0.5Fe12O19@MWCNTs nanocomposite in X-band frequency, J. Magn. Magn. Mater. 524 (2021) 167653.
[6] M.K. Naidu, K. Ramji, B.V.S.R.N. Santhosi, T.C. Shami, H.B. Baskey, B. Satyanarayana, Enhanced microwave absorption of quartic layered epoxy-MWCNT composite for radar applications, Adv. Composites Lett. 26 (2017) 133.
[7] K.R. Paton, K.A.H. Windle, Efficient microwave energy absorption by carbon nanotubes, Carbon 46 (2008) 1935.
[8] S. Bi, X.J. Su, G.L. Hou, C.H. Liu, W.L. Song, M.S. Cao, Electrical conductivity and microwave absorption of shortened multi-walled carbon nanotube/alumina ceramic composites, Ceramics Inter. 39 (2013) 5979.
[9] S. Tyagi, P. Verma, H.B. Baskey, R.C. Agarwala, V. Agarwala, T.C. Shami, Microwave absorption study of carbon nano tubes dispersed hard/soft ferrite nanocomposite, Ceramics Inter. 38 (2012) 4561.
[10] X.Y. Wang, S.C. Wei, Y. Yuan, R.B. Li, Y.J. Wang, Y. Liang, B. Wang, C.F. Dong, Effect of copper sulfide nanosphere shell on microstructure and microwave absorption properties of cobalt ferrite/carbon nanotube composites, J. Alloy. Compd. 909 (2022) 164676.
[11] L.L. Yan, L.L. Li, X.X. Ru, D.N. Wen, L. Ding, X.Y. Zhang, H.P. Diao, Y. Qin, Core-shell, wire-in-tube and nanotube structures: Carbon-based materials by molecular layer deposition for efficient microwave absorption, Carbon 173 (2021) 145.
[12] L. Wang, B. Wen, X.Y. Bai, C. Liu, H.B. Yang, NiCo Alloy/Carbon nanorods decorated with Carbon nanotubes for microwave absorption, ACS Appl. Nano Mater. 2 (2019) 7827.
[13] P.F. Yin, L.M. Zhang, X. Feng, J. Wang, J.W. Dai, Y.T. Tang, Recent Progress in ferrite microwave absorbing composites, Integr. Ferroelectr. 211 (2020) 82.
[14] Z.W. Peng, J.Y. Hwang, M. Andriese, Microwave power absorption Characteristics of ferrites, IEEE Trans. Magn. 49 (2013) 1163.
[15] A. Houbi, Z.A. Aldashevich, Y. Atassi, Z.B. Telmanovna, M. Saule, K. Kubanych, Microwave absorbing properties of ferrites and their composites: a review, J. Magn. Magn. Mater. 529 (2021) 167839.
[16] Y.J. Zhang, C.Y. Liu, X.R. Zhao, M.H. Yao, X.F. Miao, F. Xu, Enhanced microwave absorption properties of barium ferrites by Zr4+-Ni2+ doping and oxygen-deficient sintering, J. Magn. Magn. Mater. 494 (2020) 165828.
[17] F.F. Hu, H. Nan, M.Q. Wang, Y. Lin, H.B. Yang, Y. Qiu, B. Wen, Construction of core-shell BaFe12O19@MnO2 composite for effectively enhancing microwave absorption performance, Ceramics Intern. 47 (2021) 16579.
[18] A.R. Farhadizadeh, S.A.S. Ebrahimi, S.M. Masoudpanah, Magnetic and microwave absorption properties of ZnCo-substituted W-type strontium hexaferrite, J. Magn. Magn. Mater. 382 (2015) 233.
[19] J.L. Song, Y. Gao, G.G. Tan, Q.K. Man, Z. Wang, Comparative study of microwave absorption properties of ni-zn ferrites obtained from different synthesis technologies, Ceramics Intern. 48 (2022) 22896.
[20] L.A. Trusov, E.A. Gorbachev, V.A. Lebedev, A.E. Sleptsova, I.V. Roslyakov, E. S. Kozlyakova, A.V. Vasiliev, R.E. Dinnebier, M. Jansen, P.E. Kazin, Ca–Al double-substituted strontium hexaferrites with giant coercivity, Chem. Commun. 54 (5) (2018) 479–482.
[21] E.A. Gorbachev, M.V. Soshnikov, L.N. Alyabyeva, E.S. Kozlyakova, A.S. Fortuna, A. Ahmed, A.A. Eliseev, R.D. Svetogorov, L.A. Trusov, Sub-terahertz/terahertz electron resonances in hard ferrimagnets, Mater. Today 63 (2013) 99.
[22] E.A. Gorbachev, L.A. Trusov, A.E. Sleptsova, E.S. Kozlyakova, L.N. Alyabyeva, S. R. Yegiyan, A.S. Prokhorov, V.A. Lebedev, I.V. Roslyakov, A.V. Vasiliev, P.E. Kazin, Mater. Today 32 (2020) 13.
[23] E.A. Gorbachev, E.S. Kozlyakova, L.N. Alyabyeva, A. Ahmedc, L.A. Trusov, Hard ferrite magnetic insulators revealing giant coercivity and sub-terahertz natural ferromagnetic resonance at 5–300 K, Mater. Horiz. 10 (2023) 1842.
[24] E.A. Gorbachev, V.A. Lebedev, E.S. Kozlyakova, L.N. Alyabyeva, A. Ahmed, A. Cervellino, L.A. Trusov, Tuning the microstructure, magnetostatic and magnetodynamic properties of highly al-substituted M-type Sr/Ca hexaferrites prepared by citrate-nitrate auto-combustion method, Ceram. Int. 49 (16) (2023) 26411–26419.
[25] Y.-D. Chang, Y.N. Zhang, C. Meng, S.-Q. Liu, H. Chang, Z. Liu, Strong and wide microwave absorption of SrFe12−2xNixRuxO19 enhanced by dislocation stripes, Appl. Phys. Lett. 116 (2020) 082404.
[26] X.-Q. Wang, H.-Y. Yan, S.-C. Zhao, S.-Q. Liu, H. Chang, Modifiable natural ferromagnetic resonance frequency and strong microwave absorption in $BaFe_{12-y-2x}Al_ySn_xMn_xO_{19}$ M-type hexaferrite, J. Magn. Mater. Magn. 586 (2023) 171159.
[27] Yu. Xiang, N. Zhou, R. Liu, L. Wang, Xu. Zhiyi, H. Gong, T. Zhao, J. Sun, Hu. Fengxia, B. Shen, Effect of Zn2+-Sn4+ co-substitution on structural and magnetic properties of SrFe12-2xZnxSnxO19 (x = 0–2) M-type strontium ferrite, Phys. B 653 (2023) 414676.
[28] J. Tauc (F. Abeles ed.), Optical Properties of Solids, North-Holland (1972).
[29] M.M. Rhaman, M.A. Matin, M.A. Hakim, M.F. Islam, Bandgap tuning of samarium and cobalt co-doped bismuth ferrite nanoparticles, Mater. Sci. Eng. B 263 (2021) 114862.
[30] G. Fatima, I. Bibi, F. Majid, S. Kamal, S. Nouren, A. Ghafoor, Q. Raza, S.H. Al-Mijalli, Nouf Mohammad alnafisi, Munawar iqbal, mn-doped BaFe12O19 nanoparticles synthesis via micro-emulsion route: Solar light-driven photo-catalytic degradation of CV, MG and RhB dyes and antibacterial activity, Mater. Res. Bull. 168 (2023) 112491.
[31] I.A. Abdel-Latif, C. Singh, R. Joshi, A. Jasbir Singh, M.M. Gismelssed, L.-H. Alam, A.A. Ismail, M. Faisal, A.M. Asiri, I.Z. Al-Yahmadi, M.T.Z. Faten Bzour, M. M. Myint, Rahman,, Fabrication of highly sensitive 4-nitrophenol sensor and photocatalytic performance of multifunctional Ba0.5Sr0.5CoxHfxFe12-2xO19 ferrite, Mater. Chem. Phys. 288 (2022) 126396.
[32] Muhammad Yousaf, Shoaib Nazir, Qaisar Hayat, Majid Niaz Akhtar, Muhammad Akbar, Yuzheng Lu, Asma Noor, Jian-Min Zhang, M.A.K Yousaf Shah, Baoyuan Wang, Magneto-optical properties and physical characteristics of M-type hexagonal ferrite (Ba1-xCaxFe11.4Al0.6O19) nanoparticles (NPs), Ceramics International 47 (2021) 11668.
[33] E.A. Gorbachev, L.A. Trusov, M.-X. Wu, A.V. Vasiliev, R.D. Svetogorov, L. N. Alyabyeva, V.A. Lebedev, A.E. Sleptsova, M.A. Karpov, Y.M. Mozharov, B. P. Gorshunov, P.E. Kazin, Sbumicron particles of ga-substituted strontium hexaferrite obtained by a citrate auto-comustion method, J. Mater. Chem. C 9 (2021) 13832.
[34] X. Jian, B. Wu, Y. Wei, S. Dou, X. Wang, W. He, N. Mahmood, Facile synthesis of Fe3O4/GCs composites and their enhanced microwave absorption properties, ACS Appl. Mater. Interfaces 8 (2016) 6101.
[35] G. Mu, N. Chen, X. Pan, K. Yang, M. Gu, Microwave absorption properties of hollow microsphere/titania/M-type Ba ferrite nanocomposites, Appl. Phys. Lett. 91 (2007) 043110.
[36] Y. Zhu, L. Zhang, T. Natsuki, Y.-Q. Fu, Q.-Q. Ni, Facile synthesis of BaTiO3 nanotubes and their microwave absorption properties, ACS Appl. Mater. Interfaces 4, 2101 (2012) 2106.
[37] J. Singh, C. Singh, D. Kaur, S.B. Narang, R. Joshi, S. Mishra, R. Jotania, M. Ghimire, C.C. Chauhan, Tunable microwave absorption in co-al substituted M-type Ba-sr hexagonal ferrite, Mater. Design 110 (2016) 749.
[38] J. Yu, J. Yu, T. Ying, C. Cui, Y. Sun, X. Liu, The design and the preparation of mesoporous Ag_3PO_4 nanorod/$SrFe_{12}O_{19}$ hexagonal nanoflake heterostructure for excellent microwave absorption, J. Alloy. Compd. 775 (2019) 225.